STAEBLE: A surface-temperature- and avaliable-energy-based lake evaporation model

Nelson Luís Dias[1],Lucas E. B. Hoeltgebaum[2],Irani Santos[3]

[1]Federal University of Paraná (UFPR), Environmental Engineering Departament*

[2]Federal University of Paraná (UFPR), Graduate Program of Environmental Engineering

[3]Federal University of Paraná (UFPR), Geography Department

Key Points:

- A new mass transfer method for lake evaporation is proposed that self-calibrates the transfer coefficient
- The calibration is based on closing the long-term energy budget and dispenses in-situ evaporation measurements
- Standard atmospheric stability functions must be incorporated for the best results

*Current address: Rua Francisco H. dos Santos, nº 210 Centro Politécnico / Setor de Tecnologia / Departamento de Engenharia Ambiental Jardim das Américas – Curitiba PR Brazil CEP 81531-980, Caixa Postal 19011 Edifício de Administração 3º andar

Corresponding author: Nelson L. Dias, nelsonluisdias@gmail.com

Abstract

A mass transfer evaporation model is proposed that uses MODIS water surface temperature data and land-based meteorological data, and employs a new approach to calibrate the transfer coefficient via closure of the long-term energy budget of the lake. Some of the longstanding issues of developing and applying lake evaporation models are reviewed, including the adequacy of using land-based meteorological data, the difficulty of applying transfer coefficients with fixed values calibrated elsewhere, and the need to estimate rates of change of stored enthalpy when the model involves energy budget concepts. Publicly available data from a 5-year measurement campaign at Lake Mead allow to quantify the effect of using land-based data, and subsequently to test the proposed model. We show that atmospheric stability effects are very important, and that their incorporation by means of existing stability functions in the literature produces good results with a one-parameter model that can be locally calibrated with the same input data used by the model, without the need of local evaporation measurements. The model is simple in its structure and data requirements, and can be widely applied.

Plain Language Summary

The evaporation rate from a natural or artificial lake (the amount of water that is evaporated into the atmosphere in a given time, from 1 day to 1 year) is an important quantity to model and understand the weather and climate, to model the water temperature in the lake, and for water resources management in general. It is also difficult to measure, and very uncertain to estimate. We developed a model that uses simple physics based on surface water temperature measured by satellite and local meteorological measurements, and that adjusts the total evaporation over many years to be equivalent to the total energy available to convert liquid water to vapor.

1 Introduction

Natural and artificial lakes are a common part of the landscape, and essential for human life, in their multiple uses for recreation, water supply for industry, irrigation and domestic use, energy generation, etc.; they also act as "sentinels" and integrators of terrestrial and atmospheric processes (Williamson et al., 2008), and play an important role in the emission of greenhouse gases to the atmosphere (DelSontro et al., 2018). The latent and sensible heat fluxes (and attendant water vapor mass flux) between the water

surface of lakes and the atmosphere are needed as boundary conditions for atmospheric models and to quantify water losses. They are also used as boundary conditions in models for the evolution of the water temperature (see Hostetler & Bartlein, 1990), which plays a fundamental control on all biochemical processes occurring in the lake's body.

For well-known hydrological and environmental reasons, therefore, reliable lake evaporation estimates remain at the centerstage of water resources management, and even more so in the face of increased water demand and scarcity, and climate change (Veldkamp et al., 2017; Wang et al., 2018). Consequently, the need persists for reliable operational estimates of lake evaporation, *i.e.*, estimates than can use readily available environmental data and can be applied as widely as possible, at timescales ranging from daily to yearly.

It is in the nature of the underlying physical processes, however, that the best flux measurements or model-based estimates are derived from data collected directly above the water surface: the physical basis for this fact is modernly provided by Monin-Obukhov Similarity Theory (MOST) (Obukhov, 1946 1971). This is true of both the Energy-Budget Bowen Ratio Method (Bowen, 1926; Brutsaert, 1982, Chapter 10) and the Eddy Covariance Method (Swinbank, 1951; Brutsaert, 1982, Chapter 8), as well as many heat and mass transfer methods and Penman (1948)'s combination method. This experimental complicating factor is compounded, in the case of lakes, by the need to measure or estimate the rate of change of enthalpy stored in the lake's waters by means of water temperature profiles. Due to the limits in the accuracy of temperature measurements and in spatial coverage, the deeper the lake, the longer is the time interval needed to derive accurate enough estimates of change of enthalpy (Dias & Reis, 1998; Reis & Dias, 1998).

Of course, it is not impossible to perform in-lake measurements, as the early studies at lakes Hefner and Mead showed (USGS, 1954, 1958); several such studies at important lakes around the world have been conducted since then (*e.g.* Omar & El-Bakry, 1981; Assouline & Mahrer, 1993; Blanken et al., 2000; Cancelli et al., 2012; M. T. Moreo & Swancar, 2013; Armani et al., 2020). In this work, we concentrate on the particularly long 5-year data set generated by the recent USGS Lake Mead study initially reported by M. T. Moreo and Swancar (2013).

Because over-water measurements over extended periods are rare, in practice operational lake evaporation models have had to rely, at least partly, on data measured at meteorological stations over land. An early example is the hybrid method proposed by

Harbeck (1962), which combines water surface temperature and wind measured over the water with vapor pressure measured upwind on land. Harbeck proposed a mass transfer coefficient dependent on the lake's surface area. This approach was corroborated theoretically in some measure by Brutsaert and Yeh (1970). Much later, McJannet et al. (2012) compiled data for several water bodies and proposed a similar mass transfer coefficient, but with the wind measured over land. In practice, however, it appears that the mass transfer coefficient is still too dependent on local conditions for a pure mass transfer approach to be successful using a "universal" coefficient (*i.e.* a coefficient with fixed values independent of location, even with an area dependence). Most models that achieved some degree of success, therefore, relied to some extent on the energy-budget or related approaches. For instance, Kohler and Parmele (1967) adapted Penman's combination approach; Morton (1983, 1986) used the combination approach to derive a surrogate of surface water temperature (then literally impossible to obtain in practice) and use it in a slightly modified form of the Priestley-Taylor equation (Priestley & Taylor, 1972); more recently, water surface temperature has become available from remote sensing, and Zhao et al. (2020) proposed a model that uses MODIS water surface temperature data and Penman's equation, together with McJannet et al.'s mass transfer coefficient as well as Hostetler and Bartlein (1990)'s model for the evolution of water temperature profiles, to estimate the rate of change of stored enthalpy.

In all cases cited above (except for Harbeck's purely mass transfer approach), there is a need to estimate the rate of change of enthalpy by various means because continuous and sufficiently dense (in time and space) profiles of water temperature are generally not available. Moreover, although site-specific studies of turbulence over water confirm a strong dependence of mass and heat transfer coefficients on atmospheric stability (as predicted by MOST) at the scale of 30 minutes – 1 hour (*e.g.* Verburg & Antenucci, 2010; Dias & Vissotto, 2017), all operational evaporation models described above use fixed values and do not take into account atmospheric stability in the mass transfer coefficient.

In this work, we propose a different combination of physical principles. First, we use on-land meteorological data together with MODIS water surface temperature in the mass and heat transfer equations. Although there is some physical basis for this approach, provided by the Brutsaert and Yeh (1970) study, we employ it empirically (as all operational lake evaporation models are forced to do) but verify it using the recent USGS experimental campaign at lake Mead (M. T. Moreo & Swancar, 2013), showing that it

is quite reasonable in practice, even under rather extreme changes from the arid surroudings to over-water conditions. Then we investigate the extent to which net radiation estimates based on over-land data and MODIS water surface temperatures can replicate over-water measurements, and show that it is enough to use a suitably parameterized downwelling atmospheric radiation model. We propose to constrain the mass and heat transfer coefficients by imposing that the *long-term* energy budget of the lake be closed, effectively avoiding the need to calculate rates of change of enthalpy. This provides a local calibration of the mass and heat transfer coefficient, circumventing the use of a "universal" transfer coefficient with fixed parameters. Finally, we assess the performance of five versions of the approach, and show that a model that takes into account atmospheric stability via the Businger-Dyer integral Monin-Obukhov functions for momentum and scalars, and a constant "effective" surface roughness obtained from the long-term energy-budget constraint is the best choice.

2 Theory and proposed model

In this work, all symbols used should be considered daily averages unless otherwise noted. Most of the equations, however, are strictly valid at the much shorter scale of 30 minutes to 1 hour, according to MOST. The use of daily values is a compromise in the interest of simplicity and the ability to use more widely available data, but, as we shall see, atmospheric stability is still crucial at the daily time scale. In particular, care should be exercised when trying to interpret physically the turbulent scales u_*, θ_* and q_* defined below: it is better to consider them auxiliary values that, because they are derived from mixed over-land meteorological data and over-water surface temperatures at the daily timescale, do not necessarily carry their original meaning in MOST. All equations are written in the S.I. system of units; temperatures, therefore, should be entered in Kelvins. In the figures and in some temperature ranges, however, we use the auxiliary S.I. unit degree Celsius (°C).

The energy-budget equation at the water surface of the lake is

$$R_n = H + LE + D, \tag{1}$$

where R_n is the net radiation, H is the sensible heat flux, LE is the latent heat flux which is the product of $L = 2.464 \times 10^6\,\mathrm{J\,kg^{-1}}$, the latent heat of evaporation, and E, the water vapor mass flux, and D is the rate of change of enthalpy stored in the lake's wa-

ter. For simplicity, in the model L is kept constant at its nominal value at 15°C. Note that (1) implicitly neglects the ground heat flux at the lake's bottom. Net radiation is estimated from

$$R_n = R_s(1-\alpha) + \epsilon R_a - \epsilon\sigma T_0^4, \tag{2}$$

where R_s is (the directly retrieved or measured) downwelling solar radiation, α is the water's albedo, $\epsilon = 0.97$ is the water's absorptivity/emissivity, R_a is downwelling longwave radiation, $\sigma = 5.67037 \times 10^{-8}\,\mathrm{W\,m^{-2}\,K^{-4}}$ is Stefan-Boltzmann's constant, and T_0 is the water surface temperature. The daily albedo is interpolated for each day and the local latitude from Table 5 of Cogley (1979), whose values are nominally placed at the 15^{th} day of each month.

The clear-sky downwelling atmospheric radiation is estimated with Brutsaert (1975a)'s equation, *viz.*

$$R_{ac} = \epsilon_{ac}\sigma T_a^4, \qquad \epsilon_{ac} = a_B \left(\frac{e_a}{T_a}\right)^{b_B}, \tag{3}$$

where a_B and b_B are constants that vary somewhat with location. The actual downwelling atmospheric radiation is then obtained with the help of Bolz's equation (Brutsaert, 1982, Section 6.1),

$$R_a = \left(1 + 0.22C^2\right) R_{ac} \tag{4}$$

where the cloudiness C is obtained indirectly by solving for S in Prescott's (Brutsaert, 1982, Section 6.1) equation:

$$C = 1 - S, \qquad R_s = R_{se}(a_P + b_P S), \tag{5}$$

where a_P and b_P vary with location, S is sunshine duration, and R_{se} is mean daily solar radiation at the top of the atmosphere (Sellers, 1965, Chapter 3),

$$R_{se} = \left(\frac{r_a}{r}\right)^2 \frac{R_{s0}}{\pi} \left[H \sin\delta \sin\phi + \cos\delta \cos\phi \sin H\right], \tag{6}$$

where $R_{s0} = 1361.5\,\mathrm{W\,m^{-2}}$ is the solar constant, r_a is the semi-major axis of the Earth's orbit (1 astronomical unit), r is the Sun-Earth distance on a given day, ϕ is the latitude, δ is the declination of the Sun on a given day, and

$$H = \arccos(-\tan(\phi)\tan(\delta)) \tag{7}$$

is half the duration of the day in radians. For each day, r/r_a and δ are calculated from van Flandern and Pulkkinen (1979).

Here, we chose (3) on the basis of its good performance among several studies, including Sugita and Brutsaert (1993), Prata (1996), Duarte et al. (2006) and Choi et al. (2008). Note that in Sugita and Brutsaert (1993), Duarte et al. (2006) and Choi et al. (2008) the constants a_B and b_B were locally calibrated. It should also be noted that nowadays values of R_a can be retrieved from reanalysis data. Here, however, we prefer to estimate it as it would have to be if meteorological data were obtained from an actual meteorological station close to the lake.

In the proposed model, H and LE are calculated at the daily time scale from standard heat and mass transfer equations:

$$H = \rho c_p f(u,\theta)(T_0 - T_a), \tag{8}$$

$$LE = \rho c_p f(u,\theta)\frac{(e_0 - e_a)}{\gamma} = \rho L f(u,\theta)(q_0 - q_a), \tag{9}$$

where ρ is the dry air density at the nominal pressure P and temperature T of the location's altitude h in a standard atmosphere (COESA, 1976):

$$T = T_s - 0.0065h, \tag{10}$$

$$P = P_s \left[\frac{T}{T_s}\right]^{5.256}, \tag{11}$$

$$\rho = \frac{P}{R_d T}, \tag{12}$$

with $P_s = 101\,325\,\mathrm{Pa}$ and $T_s = 288.15\,\mathrm{K}$; $c_p = 1005\,\mathrm{J\,kg^{-1}K^{-1}}$ is the specific heat of dry air, $R_d = 287.038\,\mathrm{J\,kg^{-1}\,K^{-1}}$ is the dry air constant, and $\gamma = c_p P/(0.622L)$ is the psychrometric constant. We use a nominally constant ρ calculated for dry air on the grounds of simplicity, as this has little impact on the results. In (8)–(9), u is the wind speed at 10 m over land; T_a is the air temperature at 2 m over land; e_0 and q_0 are the saturation vapor pressure and specific humidity at the water surface temperature T_0; and e_a and q_a are the water vapor pressure and specific humidity at 2 m over land.

So far, equations (2)–(12) completely specify the model (assuming suitable values of a_B, b_B, a_P and b_P are provided), except for the transfer coefficient or "wind function" $f(u,\theta)$, which is assumed to be the same for H and LE; here θ is a parameter to be determined as follows. Consider a period of N days spanning an *exact* integer number of years. For example, in the dataset of this study the period goes from March 1$^{\underline{\mathrm{st}}}$ 2010 to February 28$^{\underline{\mathrm{th}}}$ 2015 and $N = 1826$ days. Then, we sum (1) over this period and impose

$$\sum_{i=1}^{N} D_i = 0 \;\Rightarrow \sum_{i=1}^{N} R_{ni} = \sum_{i=1}^{N} [H_i + LE_i]. \tag{13}$$

Using (8)–(9),

$$\sum_{i=1}^{N} R_{ni} = \sum_{i=1}^{N} \rho c_p f(u_i, \theta) \left[(T_{0i} - T_{ai}) + \frac{e_{0i} - e_{ai}}{\gamma} \right]. \tag{14}$$

The constraint (13) is reasonable, provided that total volume changes are not too drastic between the beginning and the end of the period, and that advection effects can be neglected. Otherwise, it is in principle possible to make *ad-hoc* adjustments. Then, by solving (14) for θ, we effectively calibrate a local transfer coefficient: this is one of the main results in this work. Because there is only one degree of freedom, however, only a single-parameter $f(u, \theta)$ can be prescribed. The obvious advantage is that this produces a locally-calibrated transfer coefficient that takes into account local effects in an optimal way. Another advantage is that it completely eliminates the need to estimate the problematic term D since, once θ is obtained, the transfer equations (8)–(9) can be used directly. We call the resulting model "Surface-Temperature- and Available-Energy-Based Lake Evaporation" (STAEBLE), because it uses an extremely important physical controlling variable (the surface water temperature) and ensures long-term energy conservation.

We consider 5 alternatives for $f(u, \theta)$.

STAEBLE-A:

$$f(u, \theta) = A, \tag{15}$$

where $\theta = A$ is obtained by direct substitution of (15) into (14):

$$A = \frac{\sum_{i=1}^{N} R_{ni}}{\sum_{i=1}^{N} \rho c_p \left[(T_{0i} - T_{ai}) + \frac{(e_{0i} - e_{ai})}{\gamma} \right]}. \tag{16}$$

STAEBLE-B:

$$f(u, \theta) = Bu, \tag{17}$$

where $\theta = B$ is obtained by direct substitution of (17) into (14):

$$B = \frac{\sum_{i=1}^{N} R_{ni}}{\sum_{i=1}^{N} \rho c_p u_i \left[(T_{0i} - T_{ai}) + \frac{(e_{0i} - e_{ai})}{\gamma} \right]}. \tag{18}$$

STAEBLE-AB:

$$f(u) = (A + Bu)/2, \tag{19}$$

where A and B are the previously obtained values in (16) and (18). STAEBLE-AB is an engineering compromise: because so many "Dalton-like" equations are of the form (19), we simply use the average of the previous two alternatives.

The next two alternatives are stability-dependent, and use standard MOST stability functions. For each day, one solves iteratively the following set of equations for u_*, T_*, q_*, and $\zeta_{a,b}$ (Brutsaert, 1982, Chapters 4 and 5):

$$u_* = \frac{\kappa u}{\ln\left(\frac{z_b}{z_0}\right) - \Psi_u(\zeta_b)}, \tag{20}$$

$$z_0 = a_C u_*^2/g, \tag{21}$$

$$z_{0+} = \frac{u_* z_0}{\nu}, \tag{22}$$

$$z_{0s} = z_0 \exp\left(-2.25 z_{0+}^{1/4}\right), \tag{23}$$

$$T_* = \frac{\kappa(T_0 - T_a)}{\ln\left(\frac{z_a}{z_{0s}}\right) - \Psi_s(\zeta_a)}, \tag{24}$$

$$q_* = \frac{\kappa(q_0 - q_a)}{\ln\left(\frac{z_a}{z_{0s}}\right) - \Psi_s(\zeta_a)}, \tag{25}$$

$$T_{v*} = (1 + 0.61 q_a) T_* + 0.61 T_a q_*, \tag{26}$$

$$\zeta_{a,b} = -\frac{\kappa g z_{a,b} T_{v*}}{T_{va} u_*^2}, \tag{27}$$

where the virtual temperature is $T_{va} = T_a(1+0.61q_a)$. Given a value of a_C or z_0 (fixed during the iteration), (20)–(27) (with the possible omission of (21)) are repeatedly calculated until two consecutive values of $f(u,\theta)$ in (28) below differ by less than 10^{-6} (for STAEBLE-C) or 10^{-5} (for STAEBLE-CH); see definitions below. When convergence is achieved, the transfer coefficient is

$$f(u,\theta) = \frac{\kappa^2 u}{\left[\ln\left(\frac{z_b}{z_0}\right) - \Psi_u(\zeta_b)\right]\left[\ln\left(\frac{z_a}{z_{0s}}\right) - \Psi_s(\zeta_a)\right]} \tag{28}$$

with the final values of z_0, z_{0s}, ζ_a and ζ_b.

Above, Ψ_u and Ψ_s are the Businger-Dyer integral functions for wind and a scalar (Brutsaert, 1982, section 4.2). For completeness, the equations are given in Appendix A. The reference heights are $z_a = 2\,\mathrm{m}$ for the scalars and $z_b = 10\,\mathrm{m}$ for the wind, $\kappa = 0.4$ is von Kármán's constant, $g = 9.81\,\mathrm{m\,s^{-2}}$ is the acceleration of gravity, and ζ_a and ζ_b are Obukhov's stability variable calculated at z_a and z_b respectively. The scalar roughness is calculated in (22)–(23) according to Brutsaert (1975b) assuming rough turbulent flow, where ν is the kinematic viscosity of air calculated with T from (10) according to Montgomery (1947). Strictly speaking, (23) parameterizes the water vapor roughness length, but again for the sake of simplicity we use a single value for both LE and H.

At this point, $f(u,\theta)$ is reduced to a single-parameter model, which is either an "effective" momentum roughness z_0 (we call it an effective roughness because it uses mixed

land-water variables in the transfer equations, blurring its physical meaning) or the (equally "effective") Charnock parameter a_C . We tested two alternatives:

STAEBLE-C: where $\theta = z_0$ is assumed constant, in which case (21) is omitted.

STAEBLE-CH: where $\theta = a_C$ and z_0 is calculated for each day by (21).

In both cases, the parameter θ must be obtained by trial-and-error. We use a simple bissection method (with logarithmically spaced midpoints) where either z_0 itself (in the case of STABLE-C) or a_C (in the case of STABLE-CH) is found iteratively by solving (14) for the respective θ, until $\sum_{i=1}^{N} [H_i + LE_i] / \sum_{i=1}^{N} R_{ni} < 0.01$. In STAEBLE-C, the initial interval for the search of z_0 by the bissection method is $[2 \times 10^{-8}\,\mathrm{m}, 2\,\mathrm{m}]$. In STAEBLE-CH, the initial interval for the search of a_C by the bissection method is $[2 \times 10^{-7}, 20]$.

The resulting model is parsimonius with data requirements (MODIS water surface temperature and on-land meteorological data, both at the daily time scale), calibrates the transfer coefficient $f(u, \theta)$ locally by enforcing that the long-term lake energy budget is closed without the need of local measurements of lake evaporation, and circumvents the use of the rate-of-change of enthalpy D. The simplicity of the model should make it easy to apply at any location where the required data are available. We proceed to test it at Lake Mead.

3 Test site and data

To test the proposed model, we use the publicly available data (M. Moreo, 2015) from the recent Lake Mead USGS evaporation study first reported by M. T. Moreo and Swancar (2013). Lake Mead is located in Nevada and Arizona (36.25°N, 114.39°W) and is mainly fed by the Colorado River; it has a maximum surface area of $659.3\,\mathrm{km}^2$, a maximum elevation of 374.6 m, and a total storage of $34.069\,\mathrm{Mm}^3$, being the largest American reservoir by volume, and second by area. The climate is hot and arid. For more details, see M. T. Moreo and Swancar (2013). The measured data from the study comprise 5 years of continuously reported values of daily H, LE and R_n as well as air temperature and relative humidity over the lake; and 32 months of water surface temperature at a floating platform close to Sentinel Island, from March 1$^{\mathrm{st}}$ 2010 to October 30$^{\mathrm{th}}$ 2012. The period of continuous flux measurements used here is from March 1$^{\mathrm{st}}$ 2010 to February 28$^{\mathrm{th}}$ 2015. The reported fluxes were corrected to agree more closely to independently-

measured terms of the energy-budget of the lake (M. T. Moreo & Swancar, 2013, p. 28 and Table 8). Relatively important values of heat advection at Lake Mead for the period March 2011 – February 2012 are reported, with an overall ratio of advected heat to net radiation for the first two years of measurement of $14\,\mathrm{W\,m^{-2}}/144\,\mathrm{W\,m^{-2}} \approx 10\%$ (M. T. Moreo & Swancar, 2013, Table 4). Heat advection data are not published for the whole period of measurements (5 years), however, and, as we will see, in the long run the adjusted published fluxes very closely match measured net radiation. For this reason, further consideration of heat advection is not made in this work.

For the same period and for each day, MODIS water surface temperature at 1 km resolution is available from the AQUA and TERRA satellites. For each satellite, the daily water surface temperature is taken as the mean of a daytime and a nighttime measurement. If either one or the other of the two is missing, the daily mean is filled via linear regression between the remaining value and the daily mean calculated with complete data. When both daytime and nighttime values are missing, gaps are interpolated in time. Finally, the daily water surface temperature is taken as the mean of the two satellites's temperature data. We discarded points too close to land in the MODIS grid, and averaged those closer to the center of the lake, as shown in yellow in Figure 1, to obtain a spatially representative water surface temperature. We also used a single grid point from the ERA5 reanalysis data at 31 km resolution (Hersbach et al., 2018, shown in black in Figure 1) to obtain daily time series of air temperature, water vapor pressure (both at a nominal height of 2 m), wind speed at 10 m, and solar radiation. Yang and Bright (2020) report very good values of normalized mean bias error and normalized root mean square error, of 0.93% and 14.17% respectively, for the ERA5 solar radiation product against measured values of the Baseline Surface Radiation Network station of Desert Rock, Nevada, which is approximately 131 km WNW of the Southern tip of Lake Mead.

The dataset provides a unique opportunity to verify the adequacy of several approximations inevitable in operational lake evaporation models partly based on over-land measured or retrieved data. In our case, we will be able to investigate: (i) the quality of the MODIS-derived water surface temperature compared to *in-situ* measurements; (ii) the agreement between the accumulated measured energy fluxes and net radiation, and the extent to which (13) is valid; (iii) the differences between over-land and over-water T_a and e_a; (iv) the impact of those differences on measured and estimated Bowen ratios; (v) the adequacy of net radiation derived from (3)–(5) and ultimately (vi) the ability of

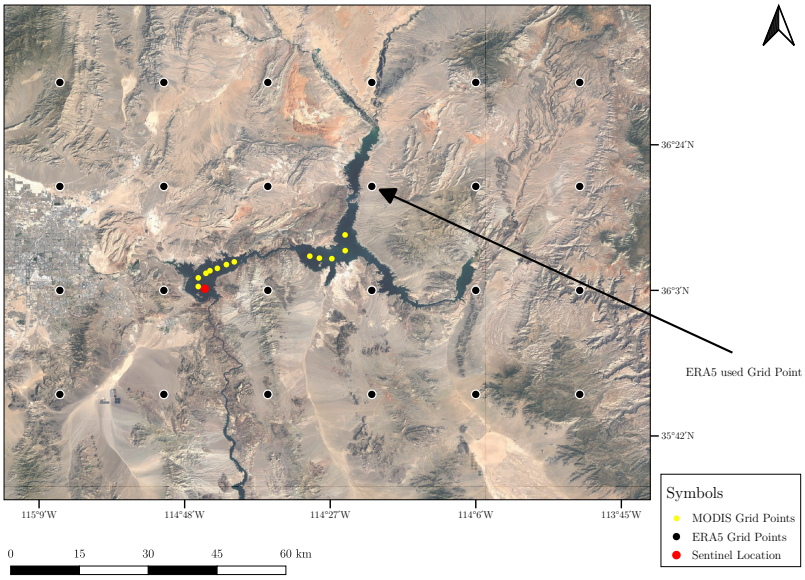

Figure 1. The retrieval of data from MODIS and ERA5 grids: black points indicate the ERA5 grid, and the arrow shows the particular grid point from which meteorological data were obtained; the yellow points are the MODIS grid points used to obtain a spatially-averaged T_0. The red point shows the location of the Sentinel Island floating platform .

the transfer equations (8)–(9) using over-land data and MODIS-derived T_0 to provide adequate estimates of E at the daily, 12-day and monthly time scales.

4 Overview of Lake Mead data

Figure 2 shows a comparison between the measured surface temperatures at the Sentinel Island platform and the MODIS estimates. We consider the MODIS temperature at the pixel closest to Sentinel Island in Figure 2-a as well as the spatially-averaged value in Figure 2-b. The two resulting T_0 values from MODIS are remarkably similar, which shows that the spatial variability of T_0 is small. Using the T_0 spatial average in STAEBLE, therefore, is unlikely to bias the results, and from this point on "MODIS T_0" means the spatially-averaged values. The overall agreement between MODIS and measured T_0 is generally good, except for the winter when MODIS tends to underestimate T_0.

Figure 3 shows the cumulative values of the measured $H + LE$ and R_n: the difference between the two is only 3%; this indicates an excellent agreement, which in no

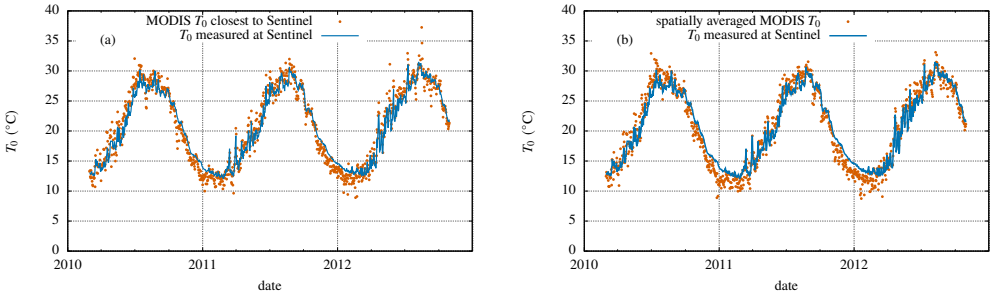

Figure 2. Comparison between measured water surface temperature and the Sentinel Island platform (blue line) versus (a) MODIS water surface temperature at the pixel closest to Sentinel and (b) spatially averaged MODIS water surface temperatures along the lake's "center".

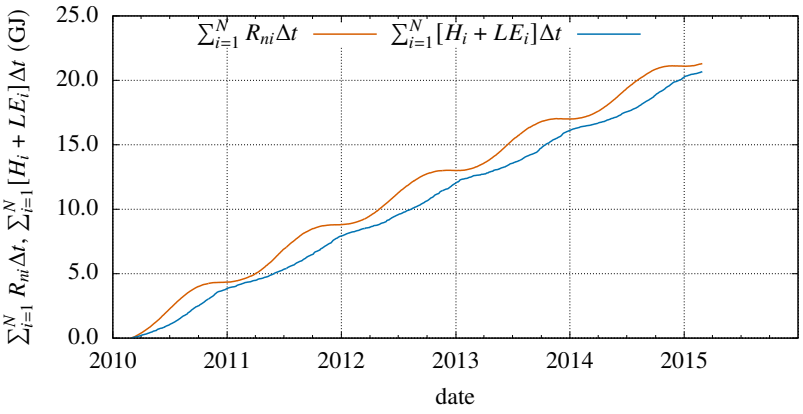

Figure 3. Cumulative values of measured H, LE and R_n.

doubt is partly due to the fact that H and LE were corrected to agree with the energy budget of the lake, as mentioned above.

A comparison between land and lake water vapor pressure and air temperature is given in figure 4. There is a substantial "lake effect" on vapor pressures, but much less on air temperatures. In hindsight, this is due to the smallness of the sensible heat flux over the lake. While the much larger water vapor flux affects the overlying air water vapor pressure significantly, it seems that the weak sensible heat fluxe is unable to produce an appreciable effect on air temperature. To the best of our knowledge, this may well be one of the longest data records available for such a comparison. This is obviously important, as it allows to quantify how much we err in lake evaporation models due to lack of over-water data, as we will now assess in terms of Bowen ratios.

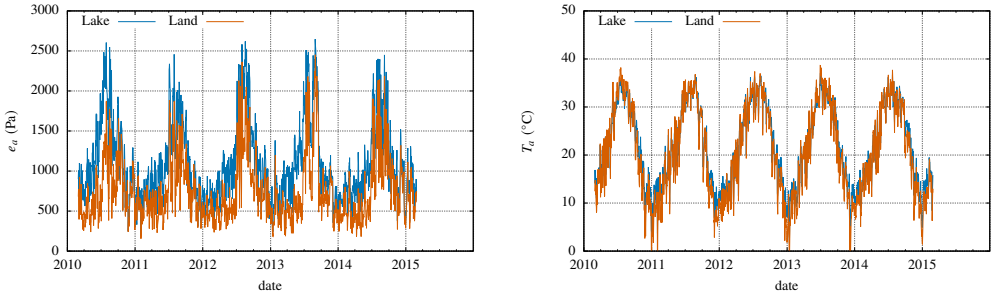

Figure 4. Comparison between lake and land values of water vapor pressure (left) and air temperature (right).

In the literature, it is sometimes expedient to differentiate between "flux" and "gradient" Bowen ratios, defined respectively by (Lang et al., 1983)

$$\mathrm{Bo}_f = \frac{H}{LE}, \qquad \mathrm{Bo}_g = \gamma \frac{T_0 - T_a}{e_0 - e_a}. \tag{29}$$

Clearly, the closer that Bo_g is to Bo_f, the better will the model partition energy between H and LE, and the better we expect our overall LE estimates to be.

Therefore, we compare Bowen ratios under two scenarios: (i) with T_0 given by the Sentinel platform measurements and (ii) with MODIS-derived T_0. Both are calculated for the common 32-month period for which Sentinel data are available, and in each case we analyze two alternatives: Bo_g from lake data *versus* Bo_f and Bo_g from land data *versus* Bo_f. The results are shown in Figure 5. The comparison of lake × land data for the calculation of Bo_g (*i.e.* (a) × (b) and (c) × (d)) is fairly reassuring: although there are obvious differences (expected in view of the results shown in Figure 4), they are not too drastic. In other words, although it introduces biases, using land data to estimate Bowen ratios still produces reasonable results. The reliability of using MODIS T_0 instead of measured T_0 at the Sentinel platform is slightly worse (*i.e.* comparing (a) with (c) and (b) with (d)), but still acceptable. The upshot is that, in spite of the caveat that according to MOST the transfer equations should be applied with in-lake measured data, the use of land-measured e_a and T_a and T_0 from MODIS at Lake Mead is still reasonable to estimate Bowen ratios and may be enough for operational purposes. This is a conclusion that applies locally only, but the fact that Lake Mead is situated in an arid region, where land-lake contrasts are expected to be larger, also lends support to the idea that the use

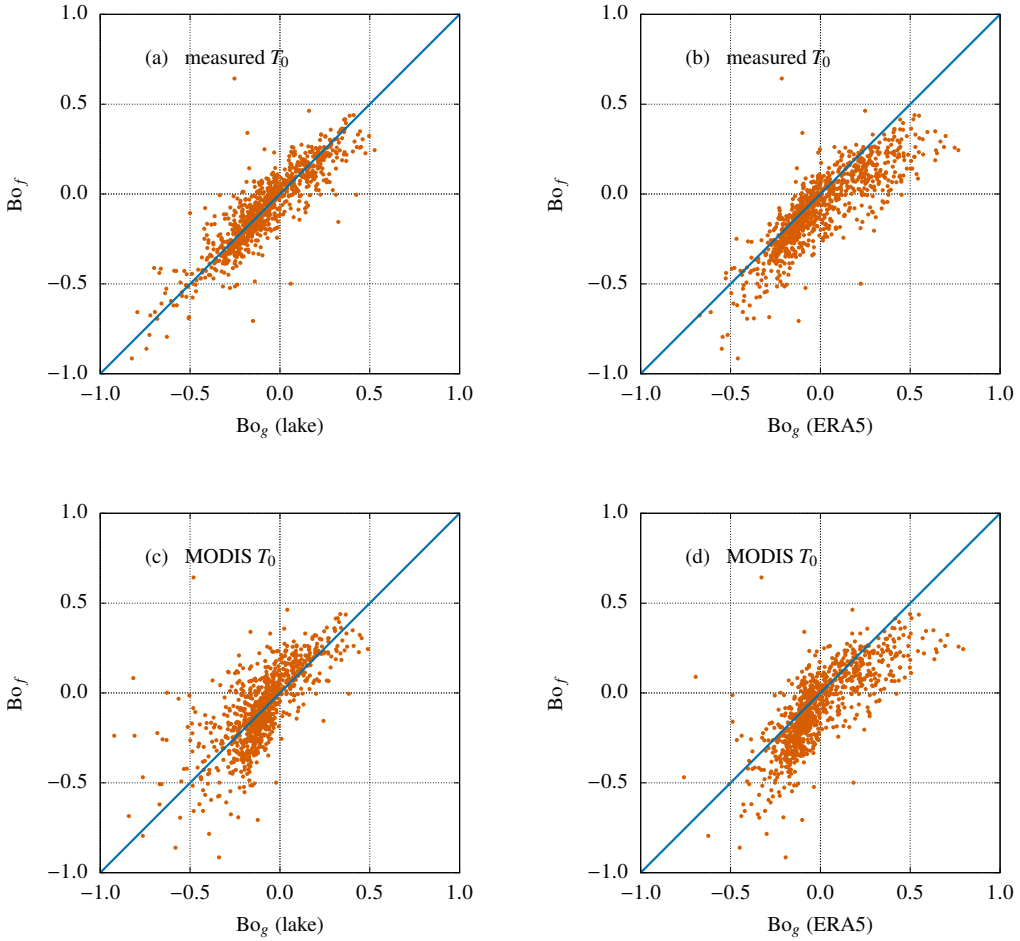

Figure 5. Comparison of Bo$_g$ × Bo$_f$. Upper row: Bo$_g$ calculated from measured T_0 and over-water e_a and T_a (a) and Bo$_g$ calculated from measured T_0 and land data e_a and T_a (b). Lower row: Bo$_g$ calculated from MODIS T_0 and over-water e_a and T_a (c) and Bo$_g$ calculated from MODIS T_0 and land data e_a and T_a (d).

of land-based air temperature and water vapor pressure may be generally acceptable in operational lake evaporation estimates.

Table 1. Values of a_B, b_B in Brutsaert (1975a)'s clear-sky atmospheric radiation equation available in the literatured and tested in this study.

Source	a_B	b_B
(Brutsaert, 1975a)	0.643	0.1428
(Sugita & Brutsaert, 1993)	0.714	0.0687
(Duarte et al., 2006)	0.625	0.1310
(Choi et al., 2008)	0.626	0.1300

5 Model validation

5.1 Atmospheric radiation

The availability of remotely-sensed water surface temperatures and the advent of automated weather stations where R_s is routinely measured (or reanalysis datasets from which it can be retrieved), leaves R_a as the most uncertain term in net radiation estimates from (2). As we mentioned above, in this work we chose to estimate R_a instead of using reanalysis-derived values (which would further simplify the model), on the grounds that the use of data from a nearby meteorological station is likely to remain a common operational practice. The choice of models and parameters is still wide, however. Here, after deciding to use Brutsaert (1975a)'s equation (3) together with (4), one must consider which values of a_B, b_B and a_P, b_P to use. We tested 3 pairs of a_B, b_B reported in the literature and listed in Table 1: the original values proposed by Brutsaert (1975a); those found by Sugita and Brutsaert (1993) with FIFE data; and those obtained by Duarte et al. (2006), which are virtually identical to the values later found by Choi et al. (2008).

The values of a_P, b_P are used to obtain S, and then C, to estimate the increase in atmospheric radiation due to the presence of clouds in (4). This of course is not the original intended use of Prescott's equation, but allows C to be obtained indirectly where manual observations are not available. Reported values of a_P, b_P are in the ranges $a_P \in [0.2, 0.3]$ and $b_P \in [0.475, 0.575]$ (Black et al., 1954; Glover & McCulloch, 1958), where we rounded the figures for simplicity. A brute-force search was made by testing, for each of the 3 pairs of a_B, b_B, 5 equally spaced values of a_P centered at 0.25, and 5 equally spaced values of b_P centered at 0.525, in a total of 75 posssibilities, by calculating R_a in (2) and comparing the resulting estimated net radiation with the measured values. Performance

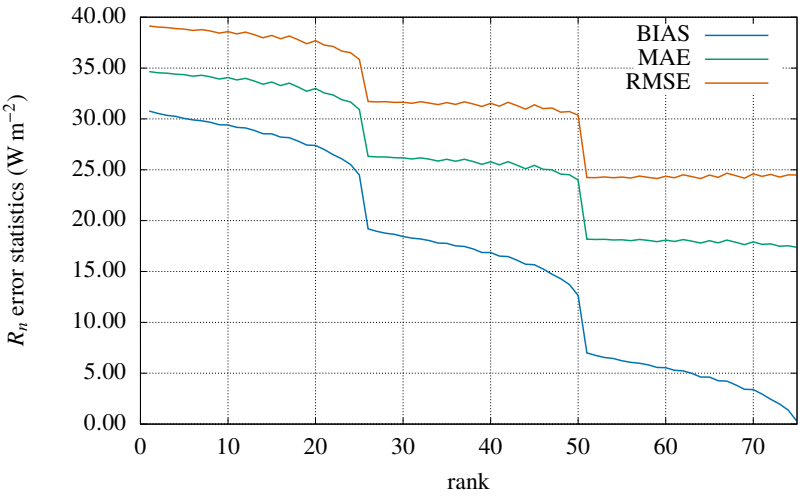

Figure 6. Error statistics of estimated net radiation as a function of model parameter choice: Bias (blue), Mean absolute error (green) and Root Mean Square Error (vermillion). The pronounced jumps indicate change in the clear-sky atmospheric radiation model parameters a_B, b_B.

statistics were calculated for each alternative: bias (BIAS), mean absolute error (MAE), root mean square error (RMSE), coefficient of correlation (r) and Willmott's refined index of model performance (d_r), which can vary from -1 to $+1$, the latter figure meaning perfect prediction (Willmott et al., 2012). The 75 values were ranked by d_r. Interestingly, the ranking is organized by the clear-sky atmospheric radiation parameters. Thus, the best 25 alternatives use Sugita and Brutsaert (1993)'s values, followed by Brutsaert (1975a)'s values. The worst 25 alternatives use Duarte et al. (2006)'s values. Therefore, the sensitivity of the error to the particular pair of a_P, b_P is relatively small. This is summarized in Figure 6, where we plot BIAS, MAE and RMSE by rank, rank 1 being the worst value of d_r and rank 75 the best. The pronounced jumps in the figure represent changes of clear-sky model parameters from each of the aformentioned 3 choices of a_B, b_B. The best set of parameters is $a_P = 0.3000$, $b_P = 0.5750$, $a_B = 0.7140$, $b_B = 0.0687$, with BIAS $= -0.26\,\mathrm{W\,m^{-2}}$, MAE $= 17.38\,\mathrm{W\,m^{-2}}$, RMSE $= 24.49\,\mathrm{W\,m^{-2}}$, $r = 0.9661$ and $d_r = 0.8961$. Note that these values were found through, and therefore reflect, the use of daily instead of 30-minute or hourly data.

In some sense, net radiation estimates remain the Achilles's heel of evaporation models based on available energy: most of these models rely on a net radiation parameter-

Table 2. The parameter θ in $f(u, \theta)$ found for each version of STAEBLE.

version	A	B	AB	C	CH
θ	A	B	$A/2$, $B/2$	z_0 (m)	a_C
	0.004210	0.001824	0.002105, 0.000912	0.008434	6.3246

ization with fixed values (*e.g.* Penman, 1948; Morton, 1983), and systematic errors in net radiation estimates will be carried over to lake evaporation estimates. In all fairness, the radiation parameterizations used in evaporation models should not be confused with the models themselves. Figure 6 gives a realistic idea of the magnitude of the errors that may be incurred if R_n estimates are not locally validated. In this work, we will adopt the best set of radiation parameters found above in the STAEBLE model evaporation estimates, thereby minimizing the errors induced by R_n estimates. It is important to note that over-water measurements of R_n are not needed for this step: it is equally possible to adjust the model with land-based measurements of R_a, as done by the aforementioned studies by Sugita and Brutsaert (1993), Duarte et al. (2006) and Choi et al. (2008); our use of R_n to obtain the best set of parameters was simply based on the fact that R_n data, instead of R_a data, were readily available.

5.2 STAEBLE model performance

The 5 versions of STAEBLE described in section 2 were tested against the measured values of the latent heat flux. For completeness, the parameter θ found by solving (14) for each version of STAEBLE is listed in Table 2. Note that z_0 and a_C are *not* representative of commonly reported over-water values, both because land-based T_a, e_a and u are used and because they are daily averages. For a comparison, using an approximate mean surface area of 370 km^2 for the first two years of study reported by M. T. Moreo and Swancar (2013, Figure 8) in Harbeck (1962)'s equation gives a constant coefficient of 0.001085 for the equivalent of B; Brutsaert (1982, Chapter 5) gives a_C in the range 0.012–0.072 from various sources; Shabani et al. (2014) however found $a_C = 0.110$. For the momentum roughness length, a typical value given by Brutsaert (1982, Chapter 5) is $z_0 = 0.00023\,\mathrm{m}$, but a recent review of the drag coefficients for lakes (Guseva et al., 2022) gives (for high wind speeds) $z_0 = 0.0013\,\mathrm{m}$.

Table 3. Error statistics for 5 versions of STAEBLE at the daily, 12-day and monthly time scales.

Time scale	Version	BIAS ($\mathrm{W\,m^{-2}}$)	MAE ($\mathrm{W\,m^{-2}}$)	RMSE ($\mathrm{W\,m^{-2}}$)	r	d_r
daily	STAEBLE-A	−2.63	54.43	73.64	0.4504	0.5363
	STAEBLE-B	+1.71	61.14	78.26	0.6628	0.4791
	STAEBLE-AB	−0.46	51.38	66.45	0.6253	0.5623
	STAEBLE-C	−4.80	46.53	62.61	0.7058	0.6035
	STAEBLE-CH	−3.00	50.50	67.86	0.7033	0.5698
12-day	STAEBLE-A	−2.64	33.44	41.34	0.7233	0.5820
	STAEBLE-B	+1.71	48.69	58.54	0.6912	0.3913
	STAEBLE-AB	−0.47	38.70	47.11	0.7222	0.5163
	STAEBLE-C	−4.81	24.41	31.47	0.8568	0.6948
	STAEBLE-CH	−3.00	26.33	34.36	0.8450	0.6708
monthly	STAEBLE-A	−2.69	29.02	35.79	0.7832	0.6063
	STAEBLE-B	+1.60	47.49	55.02	0.7036	0.3559
	STAEBLE-AB	−0.55	36.63	43.49	0.7524	0.5032
	STAEBLE-C	−4.83	20.15	25.75	0.8855	0.7267
	STAEBLE-CH	−3.03	22.44	28.24	0.8732	0.6957

The model runs at the daily time scale, after which error statistics are calculated for 3 time scales: daily, 12 days, and monthly. A LOWESS (locally weighted scatterplot smoothing) low-pass filter (Cleveland, 1979, 1981; Cleveland & Devlin, 1988) with a tri-cubic weighting function $w(x) = \left(1 - |x|^3\right)^3$ (Figueira, 2019) was applied to the daily LE data, using a window size of 21 days. Because LOWESS employs weighted linear regression, weighing more heavily the data points closest to the time at which the filtered data are calculated, this actually corresponds to a somewhat smaller *actual* time scale. Putting $\int_{-1}^{+1} w(x)\,\mathrm{d}x = 1 \times \Delta x$, where Δx is the effective scale of the independent variable, gives $\Delta x = 81/140$, which translates to a time scale of $11.57 \approx 12$ days.

The error statistics are shown in Table 3, and highlight the second main result of this work, which is the critical importance of atmospheric stability in mass transfer lake evaporation modeling. Thus, STABLE-B, which has the same analytical form of Harbeck

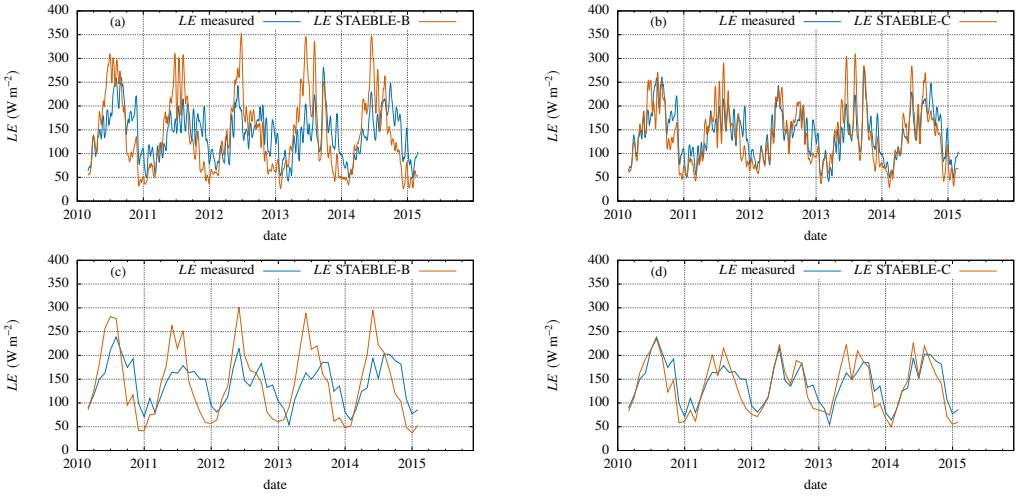

Figure 7. Comparison of the worst (STAEBLE-B) and best (STAEBLE-C) versions of the STAEBLE framework. (a) STAEBLE-B, 12-day timescale; (b) STAEBLE-C, 12-day timescale; (c) STAEBLE-B, monthly time scale and (d) STAEBLE-C, monthly time scale.

(1962)'s equation, has the largest MAE and RMSE of the 5. Moreover, its performance index d_r decreases with increasing timescale, the same happening, unsurprisingly, to STAEBLE-AB. Note that the important role of stability had already been verified with over-lake data at the 30 min – 1 h time scale by Verburg and Antenucci (2010), but now is extended to the daily time scale and over-land meteorological data. While all existing lake evaporation models for hydrological purposes (to the best of our knowledge) use a mass transfer function of the type (15), (17) or (19), with constant A and/or B, the incorporation of standard atmospheric stability effects produces a pronounced increase in overall model performance. Except for BIAS, STAEBLE-C shows the best set of performance statistics for all three time scales.

We show the worst and best versions for the 12-day and monthly time scales in Figure 7. Note that (17) and (28) share the same form (a coefficient multiplying the daily wind speed u), with the coefficient being constant in STAEBLE-B, and varying daily with atmospheric stability in STAEBLE-C: the improvement obtained by incorporating atmospheric stability into the model is again evident. Therefore, it is recommended that STAEBLE-C, which is slightly simpler than STAEBLE-CH, be adopted for operational purposes.

6 Discussion and conclusions

Perhaps the three main issues regarding lake evaporation models have been: (i) the degree of error introduced by using over-land data; (ii) the need to apply a transfer coefficient calibrated elsewhere; and (iii) the need to estimate the rate-of-change of enthalpy D. In this work, using data from Lake Mead, we have shown that (i) is not critical, and that good estimates can be obtained with land-based data. Moreover, we have introduced a new (but very simple) way to calibrate the transfer coefficient $f(u, \theta)$ by enforcing the closure of the long-run energy budget, when the cumulative value of D becomes negligible in comparison to the other terms. We emphasize that the calibration procedure does not require *in-situ* measurements of lake evaporation. We have also shown that a constant-value transfer coefficient, even if calibrated locally, although able to reproduce the average annual evaporation, performs relatively poorly at the monthly and smaller time scales. Our results show that this is caused by changes in atmospheric stability over the year. We have shown that adjusting for atmospheric stability using standard and widely accepted MOST stability functions (which do not need to be locally calibrated) solves this issue. Overall, then, (ii) is solved. The result is a model that uses a small set of data, is able to calculate H and LE with the heat and mass transfer approach (therefore dispensing with estimates of D, which solves (iii)), and is locally calibrated, which means that local effects including lake size are automatically incorporated. The model can be applied at any location where the required input data are available.

As it happens with all lake evaporation models based on available energy, good estimates of R_n impact directly on the long-term LE estimates produced by the model. It is possible to verify the quality of the R_s data and R_a estimates with simultaneous over-land measurements (or use measured data directly in the model), and this should be considered, whenever possible, for best results.

The importance of using MODIS water surface temperature data cannot be overemphasized, since STAEBLE hinges critically on them to derive its lake evaporation estimates. The small underestimation of T_0 at Lake Mead by MODIS during winter should be more closely investigated in the future.

Appendix A Adopted Businger-Dyer integral MOST functions

For stable conditions ($\zeta > 0$),

$$\Psi_s(\zeta) = \Psi_u(\zeta) = \begin{cases} -5\zeta & \zeta \leq 1, \\ -5 & \zeta > 1. \end{cases} \tag{A1}$$

For unstable conditions ($\zeta \leq 0$),

$$x = (1 - 16\zeta)^{1/4}, \tag{A2}$$

$$\Psi_u(\zeta) = 2\ln\left[\frac{(1+x)}{2}\right] + \ln\left[\frac{(1+x^2)}{2}\right] - 2\arctan(x) + \frac{\pi}{2}, \tag{A3}$$

$$\Psi_s(\zeta) = 2\ln\left[\frac{(1+x^2)}{2}\right]. \tag{A4}$$

Open Research

All input data used in this research are publicly available at the ERA5 repository according to the licence to use Copernicus Products (Hersbach et al., 2018), the AQUA and TERRA MODIS repositories (Wan et al., 2021a, 2021b) and the USGS Lake Mead Study data repository (M. Moreo, 2015). The processed data are available at Dias et al. (2022).

Acknowledgments

We are deeply grateful to the USGS and all USGS personnel involved in the Lake Mead 2010–2015 study whose data are used herein, without which this research would not have been possible.

This study was funded by FUNPAR research grants, 03638 e 03955, both funded by the Brazilian Agência Nacional de Águas (National Water Agency), ANA.

We thank Henrique F. Duarte for his careful reading of the manuscript and many suggestions that helped to improve it.

References

Armani, F. A. S., Dias, N. L., & Damázio, J. M. (2020). Eddy-covariance CO_2 fluxes over Itaipu Lake, southern brazil. *Rev Bras Rec Hídr*, *25*, 1–14.

Assouline, S., & Mahrer, Y. (1993). Evaporation from lake Kineret 1. Eddy correlation system measurements and energy budget estimates. *Water Resour Res*,

29(4), 901–910.

Black, J., Bonython, C., & Prescott, J. (1954). Solar radiation and the duration of sunshine. *Q J R Meteorol Soc*, *80*(344), 231–235.

Blanken, P. D., Rouse, W. R., Culf, A. D., Spence, C., Boudreau, L. D., Jasper, J. N., ... Verseghy, D. (2000). Eddy covariance measurements of evaporation from Great Slave Lake, Northwest Territories, Canada. *Water Resour Res*, *36*(4), 1069–1077.

Bowen, I. S. (1926). The ratio of heat losses by conduction and by evaporation from any water surface. *Phys Rev*, *27*, 779–787.

Brutsaert, W. (1975a). On a derivable formula for long-wave radiation from clear skies. *Water Resour Res*, *11*, 742–744.

Brutsaert, W. (1975b). The roughness length for water vapor, sensible heat and other scalars. *J Atmos Sci*, *32*, 2028–2031.

Brutsaert, W. (1982). *Evaporation into the atmosphere.* Dordrecht: D. Reidel. (309 pp.)

Brutsaert, W., & Yeh, G.-T. (1970). Implications of a type of empirical evaporation formula for lakes and pans. *Water Resour Res*, *6*, 1202–1209.

Cancelli, D. M., Dias, N. L., & Chamecki, M. (2012). Dimensionless criteria for the production-dissipation equilibrium of scalar fluctuations and their implications for scalar similarity. *Water Resour Res*, *48*, W10522. doi: 10.1029/2012WR012127

Choi, M., Jacobs, J. M., & Kustas, W. P. (2008). Assessment of clear and cloudy sky parameterizations for daily downwelling longwave radiation over different land surfaces in florida, usa. *Geophys Res Lett*, *35*(20).

Cleveland, W. S. (1979). Robust locally weighted regression and smoothing scatterplots. *J Am Stat Assoc*, *74*(368), 829–836.

Cleveland, W. S. (1981). Lowess: A program for smoothing scatterplots by robust locally weighted regression. *Am Stat*, *35*(1), 54.

Cleveland, W. S., & Devlin, S. J. (1988). Locally weighted regression: an approach to regression analysis by local fitting. *J Am Stat Assoc*, *83*(403), 596–610.

COESA. (1976). *U.S. Standard Atmosphere, 1976.* (Tech. Rep.). U.S. Government Printing Office.

Cogley, J. G. (1979). The albedo of water as a function of latitude. *Mon Wea Rev*,

107(6), 775–781.

DelSontro, T., Beaulieu, J. J., & Downing, J. A. (2018). Greenhouse gas emissions from lakes and impoundments: Upscaling in the face of global change. *Limnol Oceanogr Lett*, *3*(3), 64–75.

Dias, N. L., Hoeltgebaum, L. E. B., & Santos, I. (2022). *Dataset for 'STAEBLE: A surface-temperature- and avaliable-energy-based lake evaporation model' article, HydroShare.* Retrieved from `https://doi.org/10.4211/hs.fa49d7f16703447b9e04552cc532936d` doi: 10.4211/hs.fa49d7f16703447b9e04552cc532936d

Dias, N. L., & Reis, R. J. (1998). Métodos de cálculo do balanço de entalpia em lagos e erros associados (in Portuguese). *Rev Bras Rec Hídr*, *3*(3), 45–56.

Dias, N. L., & Vissotto, D. (2017). The effect of temperature-humidity similarity on bowen ratios, dimensionless standard deviations, and mass transfer coefficients over a lake. *Hydrol Process*, *31*(2), 256–269. Retrieved from `http://dx.doi.org/10.1002/hyp.10925` doi: 10.1002/hyp.10925

Duarte, H. F., Dias, N. L., & Maggiotto, S. R. (2006). Assessing daytime downward longwave radiation estimates for clear and cloudy skies in Southern Brazil. *Agric For Meteorol*, *139*, 171–181. doi: 10.1016/j.agrformet.2006.06.008

Figueira, J. P. (2019). *LOESS smoothing data using local regression.* Retrieved from `https://towardsdatascience.com/loess-373d43b03564`

Glover, J., & McCulloch, J. (1958). The empirical relation between solar radiation and hours of sunshine. *Q J R Meteorol Soc*, *84*(360), 172–175.

Guseva, S., Armani, F., Desai, A., Dias, N. L., Eugster, W., Iwata, H., ... Lorke, A. (2022). Bulk transfer coefficients estimated from eddy-covariance measurements over lakes and reservoirs. *Submitted to J Geophys Res*.

Harbeck, G. E., Jr. (1962). *A practical field technique for measuring reservoir evaporation utilizing mass-transfer theory* (Professional Paper Nos. 272–E). U. S. Geological Survey. Available at `https://pubs.usgs.gov/pp/0272e/report.pdf`.

Hersbach, H., Bell, B., Berrisford, P., Biavati, G., Horányi, A., Muñoz Sabater, J., ... Thépaut, J.-N. (2018). *ERA5 hourly data on single levels from 1979 to present. Copernicus Climate Change Service (C3S) Climate Data Store (CDS).* [dataset]. Retrieved from `https://cds.climate.copernicus.eu/`

cdsapp#!/dataset/reanalysis-era5-single-levels?tab=form doi: 10.24381/cds.adbb2d47

Hostetler, S. W., & Bartlein, P. J. (1990, October). Simulation of lake evaporation with application to modeling lake level variations of Harney-Malheur Lake, Oregon. *Water Resour Res*, *26*(10), 2603-2612.

Kohler, M., & Parmele, L. (1967). Generalized estimates of free-water evaporation. *Water Resour Res*, *3*, 997–1005.

Lang, A., Mcnaughton, K., Fazu, C., Bradley, E., & Ohtaki, E. (1983). Inequality of eddy transfer coefficients for vertical transport of sensible and latent heats during advective inversions. *Boundary-Layer Meteorol*, *25*, 25–41.

McJannet, D. L., Webster, I. T., & Cook, F. J. (2012). An area-dependent wind function for estimating open water evaporation using land-based meteorological data. *Environ Modell Softw*, *31*, 76–83.

Montgomery, R. B. (1947). Viscosity and thermal conductivity of air and diffusivity of water vapor in air. *J of Meteorology*, *4*, 193–196.

Moreo, M. (2015). *Evaporation data from Lake Mead and Lake Mohave, Nevada and Arizona, March 2010 through April 2015* [U.S. Geological Survey Data Release]. Retrieved from http://dx.doi.org/10.5066/F79C6VG3

Moreo, M. T., & Swancar, A. (2013). *Evaporation from Lake Mead, Nevada and Arizona, March 2010 through February 2012* (Scientific Investigations Report No. 2013-5229). Reston, Virginia: U.S. Geological Survey.

Morton, F. I. (1983). Operational estimates of lake evaporation. *J Hydrol*, *66*, 77–100.

Morton, F. I. (1986). Practical estimates of lake evaporation. *J Appl Meteorol*, *25*, 371–387.

Obukhov, A. M. (1946 1971). Turbulence in an atmosphere with non-uniform temperature. *Boundary-Layer Meteorol*, *2*, 7–29.

Omar, M., & El-Bakry, M. (1981). Estimation of evaporation from the lake of the aswan high dam (lake nasser) based on measurements over the lake. *Agr Forest Meteorol*, *23*, 293–308.

Penman, H. (1948). Natural evaporation from open water, bare soil and grass. *P Roy Soc London*, *A*(193), 120–146.

Prata, A. J. (1996). A new long-wave formula for estimating downward clear-sky ra-

diation at the surface. *Q J Roy Meteorol Soc*, *122*, 1127–1151.

Priestley, C. H. B., & Taylor, R. J. (1972). On the assessment of surface heat flux and evaporation using large scale parameters. *Monthly Weather Review*, *100*(2), 80–92.

Reis, R. J., & Dias, N. L. (1998). Multi-season lake evaporation: energy-budget estimates and CRLE model assessment. *J Hydrol*, *208*, 135-147. Retrieved from https://doi.org/10.1016/S0022-1694(98)00160-7 doi: 10.1016/S0022-1694(98)00160-7

Sellers, W. D. (1965). *Physical climatology.* Chicago: The University of Chicago Press.

Shabani, B., Nielsen, P., & Baldock, T. (2014). Direct measurements of wind stress over the surf zone. *J Geophys Res-Oceans*, *119*, 2949–2973.

Sugita, M., & Brutsaert, W. (1993). Cloud effect in the estimation of instantaneous downward longwave radiation. *Water Resour Res*, *29*(3), 599-605.

Swinbank, W. C. (1951). Measurement of vertical transfer of heat and water vapor by eddies in the lower atmosphere. *J Meteorol*, *8*, 135–145.

USGS. (1954). *Water-loss investigations: Lake hefner studies* (Geol. Surv. Prof. Paper No. 269). U. S. Geological Survey.

USGS. (1958). *Water-loss investigations: Lake mead studies* (Geol. Surv. Prof. Paper No. 298). U. S. Geological Survey.

van Flandern, T. C., & Pulkkinen, K. F. (1979, November). Low-precision formulae for planetary positions. *Astrophys J SupplS*, *41*, 391-411. doi: 10.1086/190623

Veldkamp, T., Wada, Y., Aerts, J., Döll, P., Gosling, S. N., Liu, J., ... others (2017). Water scarcity hotspots travel downstream due to human interventions in the 20th and 21st century. *Nat Commun*, *8*(1), 1–12.

Verburg, P., & Antenucci, J. P. (2010). Persistent unstable atmospheric boundary layer enhances sensible and latent heat loss in a tropical great lake: Lake Tanganyika. *J Geophys Res-Atmos*, *115*(D11), D11109. Retrieved from http://dx.doi.org/10.1029/2009JD012839 doi: 10.1029/2009jd012839

Wan, Z., Hook, S., & Hulley, G. (2021a). *MODIS/Aqua Land Surface Temperature/Emissivity Daily L3 Global 1km SIN Grid V061* [dataset]. Retrieved from https://doi.org/10.5067/MODIS/MYD11A1.061 (NASA EOSDIS Land Pro-

654 cesses DAAC) doi: 10.5067/MODIS/MYD11A1.061
655 Wan, Z., Hook, S., & Hulley, G. (2021b). *MODIS/Terra Land Surface Tempera-*
656 *ture/Emissivity Daily L3 Global 1km SIN Grid V061* [dataset]. Retrieved from
657 `https://doi.org/10.5067/MODIS/MOD11A1.061` (NASA EOSDIS Land Pro-
658 cesses DAAC) doi: 10.5067/MODIS/MOD11A1.061
659 Wang, W., Lee, X., Xiao, W., Liu, S., Schultz, N., Wang, Y., ... Zhao, L. (2018).
660 Global lake evaporation accelerated by changes in surface energy allocation in
661 a warmer climate. *Nat Geosci*, *11*(6), 410–414.
662 Williamson, C. E., Dodds, W., Kratz, T. K., & Palmer, M. A. (2008). Lakes and
663 streams as sentinels of environmental change in terrestrial and atmospheric
664 processes. *Front Ecol Environ*, *6*(5), 247–254.
665 Willmott, C. J., Robeson, S. M., & Matsuura, K. (2012). A refined index of model
666 performance. *International Journal of Climatology*, *32*(13), 2088–2094.
667 Yang, D., & Bright, J. M. (2020). Worldwide validation of 8 satellite-derived and re-
668 analysis solar radiation products: A preliminary evaluation and overall metrics
669 for hourly data over 27 years. *Sol Energy*, *210*, 3–19.
670 Zhao, G., Gao, H., & Cai, X. (2020). Estimating lake temperature profile and evap-
671 oration losses by leveraging MODIS LST data. *Remote Sen Environ*, *251*,
672 112104.